Submitted April 7, 2000; Accepted June 28, 2000; to appear in ApJ Dec. 1, 2000
Preprint typeset using LaTeX style emulateapj v. 04/03/99

THE X-RAY SIZE-TEMPERATURE RELATION FOR INTERMEDIATE REDSHIFT GALAXY CLUSTERS

Joseph J. Mohr[1,2], Erik D. Reese[2], E. Ellingson[3], Aaron D. Lewis[3] & August E. Evrard[4]

Submitted April 7, 2000; Accepted June 28, 2000; to appear in ApJ Dec. 1, 2000

ABSTRACT

We present the first measurements of the X-ray size-temperature (ST) relation in intermediate redshift ($z \sim 0.30$) galaxy clusters. We interpret the local ST relation ($z \sim 0.06$) in terms of underlying scaling relations in the cluster dark matter properties, and then we use standard models for the redshift evolution of those dark matter properties to show that the ST relation does not evolve with redshift. We then use ROSAT HRI observations of 11 clusters to examine the intermediate redshift ST relation; for currently favored cosmological parameters, the intermediate redshift ST relation is consistent with that of local clusters. Finally, we use the ST relation and our evolution model to measure angular diameter distances; with these 11 distances we evaluate constraints on Ω_M and Ω_Λ which are consistent with those derived from studies of Type Ia supernovae. The data rule out a model with $\Omega_M = 1$ and $\Omega_\Lambda = 0$ with 2.5σ confidence. When limited to models where $\Omega_M + \Omega_\Lambda = 1$, these data are inconsistent with $\Omega_M = 1$ with 3σ confidence.

Subject headings: galaxies: clusters: general — intergalactic medium — cosmology

1. INTRODUCTION

Nearby galaxy clusters exhibit a tight correlation between X-ray isophotal size and emission weighted intracluster medium (ICM) temperature (Mohr & Evrard 1997; hereafter ME97). This correlation is evidence of regularity; it exists in an X-ray flux limited sample of 45 clusters (Edge et al. 1990), where no attempt has been made to use the X-ray morphologies to exclude clusters showing signatures of recent, major mergers. The scatter around the X-ray size–temperature (ST) relation is approximately 15% in size, comparable to the scatter of elliptical and lenticular galaxies around their fundamental plane (Jørgensen, Franx & Kjærgaard 1996). This small scatter in the galaxy cluster scaling relation is intriguing, because (1) there is overwhelming evidence that galaxy clusters are still accreting mass (e.g. Mohr et al. 1995, Buote & Tsai 1996) and (2) elliptical galaxies are generally thought to be among the most regular objects in the universe.

ME97 use 48 N-body and hydrodynamical simulations of cluster formation in four different cosmological models to address this apparent contradiction between regularity and ongoing accretion in nearby clusters. Using simulations from both $\Omega_M = 0.3$ and $\Omega_M = 1$ cosmologies, they show that a tight ST relation is expected even in cosmogonies where there is significant cluster growth at the present epoch.

The high degree of regularity implied by the ST relation is surprising, because the well known correlation between X-ray luminosity and emission weighted mean temperature (the $L_X - T_X$ relation) has very large scatter (David et al. 1993). ME97 show that the same cluster ensemble which exhibits a 15% scatter in the ST relation exhibits a 52% scatter in L_X around the $L_X - T_X$ relation. This higher scatter in the $L_X - T_X$ relation results from the sensitivity of the X-ray luminosity to the densest regions of the cluster– a sensitivity to the presence or absence of so-called cooling flows (Fabian et al. 1994). This interpretation is supported by more recent work where cluster ensembles specially chosen to contain no cooling flow clusters conform to $L_X - T_X$ relations with significantly reduced scatter of 25% (Arnaud & Evrard 1999). Additionally, when central parts of cooling flow clusters are excluded, the scatter in the $L_X - T_X$ relation decreases (Markevitch 1998).

Finally, cluster regularity is also evident in the tight correlation between ICM mass and emission weighted temperature (the $M_{ICM} - T_X$ relation). When measuring ICM mass within a limiting radius of r_{500} (the radius where the enclosed overdensity is 500 times the critical density) the scatter in mass about the $M_{ICM} - T_X$ relation is 17% (Mohr, Mathiesen & Evrard 1999). Observational studies of the ST relation followed by work on the $L_X - T_X$ and $M_{ICM} - T_X$ relations support a scenario where clusters exhibit regularity similar to that of elliptical galaxies in the properties measured on the scales of their virial regions, but exhibit significant irregularities in the properties of the densest, central regions where physical processes other than gravity and gas dynamics– such as radiative cooling and magnetic fields– play significant roles (Mohr & Evrard 1997, Arnaud & Evrard 1999, Mohr, Mathiesen & Evrard 1999). The evidence indicating cluster regularity is balanced by evidence for departures from regularity; the scatter in the observed scaling relations is larger than can be accounted for by the measurement uncertainties. This resolved scatter contains clues about, among other things, cluster peculiar velocities and departures from equilibrium.

[1]Chandra Fellow
[2]Department of Astronomy and Astrophysics, University of Chicago, Chicago, IL
[3]Department of Astronomy, University of Colorado, Boulder, CO
[4]Department of Physics, University of Michigan, Ann Arbor, MI

Here we examine the ST relation at intermediate redshift ($0.19 \leq z \leq 0.55$) using ROSAT HRI observations of the Canadian Network for Observational Cosmology (CNOC; e.g. Yee et al. 1996, Lewis et al. 1999) cluster sample. The ST relation provides a potentially powerful tool to study the expansion history of the universe. As explained in detail below, the ST relation is rather insensitive to cosmological evolution. Thus, armed with an accurate model of cluster evolution, one could use the ST relation to measure distances at intermediate redshift, constraining the deceleration parameter q_0.

We first present the X-ray ST relation in the nearby cluster sample (§2) and then present an interpretation of the ST relation in terms of regularity in the underlying dark matter properties of the cluster. Section 3 describes observations of the ST relation in intermediate redshift clusters. In §3.3 we use these observations to constrain cosmological parameters. Section 4 contains a summary of our conclusions. Throughout the paper we use $H_0 = 50h_{50}$ km/s/Mpc.

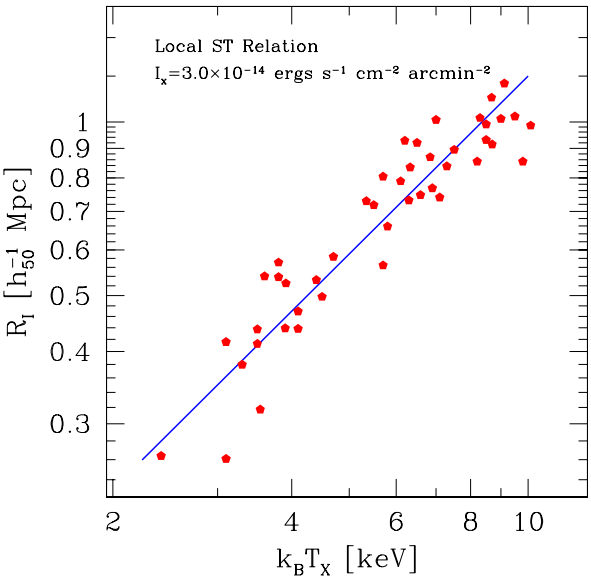

FIG. 1.— The X-ray isophotal size versus emission weighted mean ICM temperature T_X for an X-ray flux limited sample of 45 nearby clusters. We use the isophote $I = 3.0 \times 10^{-14}$ erg/s/cm^2/arcmin^2 within the cluster rest frame 0.5:2.0 keV band. The solid line represents the best fit relation, and the RMS scatter about this line is 15% in size.

2. LOCAL X-RAY ST RELATION

Below we present observations of the ST relation in an X-ray flux limited sample of clusters and then discuss cluster scaling relations.

2.1. *Observations*

Fig 1 contains a plot of the X-ray ST relation for an ensemble of nearby galaxy clusters (see ME97 for cluster list). This sample is essentially a low redshift sample, $z_{median} \sim \langle z \rangle = 0.055$ with RMS variation $\sigma_z = 0.03$, but the full redshift range is $0.01 \leq z \leq 0.19$. The cluster isophotal size R_I is plotted versus the emission weighted mean ICM temperature T_X, where

$$R_I = \sqrt{A_I/\pi} \tag{1}$$

and A_I is the area enclosed by the isophote I. The isophotal size is a model-independent measure extracted directly from the X-ray image. ICM temperatures come from the literature (listed in ME97). In this figure we use the galactic absorption corrected surface brightness $I = 3.0 \times 10^{-14}$ ergs s^{-1}cm^{-2}arcmin^{-2} within the cluster rest frame 0.5-2.0 keV band. In the conversion from count rate to physical flux units we use PROS, assume a Raymond-Smith spectrum with the published mean temperature T_X and $\frac{1}{3}$ cosmic abundances (Mushotzky & Loewenstein 1997). We convert between the angular size and physical size of the isophotal region using the angular diameter distance, and we also correct I for cosmological dimming $(1+z)^4$.

The best fit power law to this local ST relation has the form

$$R_I = (0.71 \pm 0.02) \left(\frac{T_X}{6\,\mathrm{keV}}\right)^{1.02\pm0.11} h_{50}^{-1}\ \mathrm{Mpc} \tag{2}$$

and the scatter about this relation is 15% in R_I. This fit is shown as a solid line in Fig 1. Because this is the local ST relation, it is only weakly dependent on the deceleration parameter. For this relation we have assumed the parameters $\Omega_M = 0.3$ and $\Omega_\Lambda = 0.7$; for $\Omega_M = 0.3$ and $\Omega_\Lambda = 0$ the normalization is 1.8% lower, and for $\Omega_M = 1$ the normalization is 2.7% lower.

2.2. *Cluster Scaling Relations*

Galaxy cluster scaling relations between, for example, virial mass and temperature T are expected if clusters are approximately virialized. The spherical collapse model predicts that newly collapsed objects will have mean densities which are Δ times the critical density $\rho_{crit} = 3H^2/8\pi G$, where H is the Hubble parameter and in an Einstein-de Sitter model $\Delta = 18\pi^2$. Therefore, we define the virial radius r_Δ of an object with virial mass M_Δ to be

$$r_\Delta = \left(\frac{M_\Delta}{\frac{4}{3}\pi\Delta\rho_{crit}}\right)^{1/3}. \tag{3}$$

Newly collapsed clusters may also satisfy the virial relation

$$GM_\Delta = aTr_\Delta \tag{4}$$

where T is the virial temperature and a is a number dependent on the cluster density and temperature structure; in the case that cluster structure is self similar (i.e. that massive clusters are simply rescaled versions of low mass clusters) a will be constant for all T and Eqns 3 and 4 lead to the well known scaling relations between virial mass, radius and temperature

$$M_\Delta = \frac{(a'T)^{\frac{3}{2}}}{\sqrt{\Delta\rho_{crit}}} \text{ and } r_\Delta = \frac{(a'T)^{\frac{1}{2}}}{\sqrt{\Delta\rho_{crit}}}, \tag{5}$$

where a' is a dimensionless structure parameter like a. These scaling relations are expected to hold for a range of r_δ and M_δ, where r_δ is the region with enclosed overdensity δ with respect to ρ_{crit} and M_δ is the corresponding enclosed mass. Numerical cluster simulations indicate that the emission weighted mean ICM temperature T_X is an adequate proxy for the virial temperature T, and that these

scaling relations exist even in cluster populations which exhibit merging and substructure (Evrard, Metzler & Navarro 1996, Bryan & Norman 1998). Using simulations to normalize these relations, one finds that clusters with T_X of 10 keV have virial masses $M_{200} = 4 \times 10^{15} h_{50}^{-1} M_\odot$ and virial radii $r_{200} = 4 h_{50}^{-1} Mpc$. The small scatter in the observed ST relation, the correlation between ICM mass and temperature (see Section 1), and a direct study of the correlation between binding mass (estimated using cluster galaxy kinematics) and emission weighted temperature (Horner, Mushotzky & Scharf 1999) provide evidence that the conditions required for Eqn 5 to be valid are generally met in real galaxy clusters.

2.3. *X-ray ST Relation*

The X-ray surface brightness (units: ergs $s^{-1} cm^{-2} sr^{-1}$) at a projected radius R_δ from the cluster center is

$$I(R_\delta) = \frac{1}{2\pi\,(1+z)^4} \int_0^\infty dl\, n_e(r) n_H(r) \Lambda(T) \qquad (6)$$

where n_e and n_H are the electron and proton number densities, $r = \sqrt{R_\delta^2 + l^2}$ is the distance from the cluster center and $\Lambda(T)$ is the X-ray emission coefficient which includes contributions from thermal bremsstrahlung and line emission (Raymond & Smith 1977). We can express the ICM density ρ_g in terms of the underlying dark matter density ρ_{dm}: $\rho_g(r) = f_g \rho_{dm}(r) g(r)$, where f_g is the ICM mass fraction within the virial region and $g(r)$ is a function describing differences in the dark matter and ICM density distributions; then, using $n_i = \rho_g / \mu_i m_p$, we can rewrite the X-ray surface brightness as

$$I(R_\delta) = \frac{f_g^2 \Lambda(T_X)}{2\pi m_p^2 \mu_e \mu_H\,(1+z)^4} \int_0^\infty dl\, \rho_{dm}^2(r) g^2(r) \qquad (7)$$

We bring the emission coefficient out of the integral and use the value at $T = T_X$; although this is only strictly valid for an isothermal gas, the temperature insensitivity of $\Lambda(T)$ band limited to 0.5:2.0 keV makes this an excellent approximation even in the presence of departures from isothermality (e.g. Fabricant, Lecar & Gorenstein 1980, Mohr, Mathiesen & Evrard 1999).

Finally, we express the dark matter density profile in terms of the characteristic overdensity of the virial region: $\rho_{dm}(r) = \Delta \rho_{crit} f_{dm}(r_\Delta y)$, where $f_{dm}(y)$ encodes the dependence of the dark matter profile on a dimensionless radius $y = r/r_\Delta$; this approach is consistent with numerical cluster simulations, which indicate that cluster dark matter density profiles have a "universal" form (Navarro, Frenk & White 1997, hereafter NFW). More recently, higher resolution simulations have shown differences between the inner profile (at radii which are 1% of the virial radius) and the form proposed by NFW (Moore et al. 1999, Jing & Suto 1999); these differences appear to be smallest for cluster scale haloes, and none of our conclusions are sensitive to the behavior of the density profile at 1% of the virial radius. Expressing ρ_{dm} in this way, and removing the characteristic scale R_δ from the integral, the X-ray surface brightness becomes

$$I(R_\delta) = \frac{f_g^2 \Lambda(T) \rho_{crit}^2 \Delta^2 R_\delta}{2\pi m_p^2 \mu_e \mu_H\,(1+z)^4} \Theta \qquad (8)$$

where Θ is a dimensionless integral which encodes the shape of the ICM density profile: $\Theta = \int_0^\infty d\lambda\, f_{dm}^2(\eta) g^2(\eta)$, where $\eta = \sqrt{1+\lambda^2}$ and $\lambda^2 = (r/R_\delta)^2 - 1$.

We relate R_δ and R_I using the shape of the typical X-ray surface brightness profile; $I(R)$ is typically well fit by the so-called β model (Cavaliere & Fusco-Femiano 1978)

$$I(R) = I_0 \left(1 + \left(\frac{R}{R_c}\right)^2\right)^{-3\beta+1/2} \qquad (9)$$

where R_c is the core radius; well outside the core the surface brightness falls as $I(R) \propto R^{1-6\beta}$. Therefore we write

$$R_I = R_\delta \left(\frac{I(R_\delta)}{I}\right)^{1/(6\beta-1)}. \qquad (10)$$

Using Eqn. 5 to substitute T_X for R_δ, one can readily determine the ST relation at a particular redshift in the case that cluster structure is self similar

$$R_I \propto T_X^\alpha \,\text{where}\, \alpha = \frac{3\beta}{6\beta - 1} \qquad (11)$$

For $\beta = 2/3$, a typical observed value (Jones & Forman 1984, Mohr, Mathiesen & Evrard 1999), the predicted ST relation has $\alpha = 2/3$, shallower than the observed relation: $\alpha = 1.02 \pm 0.11$. The observed increase in ICM mass fraction f_g with cluster temperature T_X (Mohr, Mathiesen & Evrard 1999) is enough to explain the steepness of the observed relation. The physics underlying this systematic variation in cluster gas mass fraction is likely heating of the intergalactic medium during the process of galaxy formation. This so-called preheating affects the structure of the gas in low mass clusters more so than in high mass clusters (e.g. Metzler & Evrard 1994, Cavaliere, Menci & Tozzi 1998, Ponman, Cannon & Navarro 1999). As discussed below, in comparing the local and intermediate redshift ST relations it is important only that the effects of this preheating be similar in both samples.

3. INTERMEDIATE REDSHIFT X-RAY ST RELATION

Before presenting the intermediate redshift ST relation, we present an evolution model and our measurement methods.

3.1. *Evolution of the ST Relation*

Comparison of ST relations in nearby and distant populations requires a model for how the expected changes in cluster structure with increasing redshift will affect the ST relation. In the previous section we presented an explanation of the correlation between cluster X–ray isophotal size and emission weighted ICM temperature T_X as a manifestation of underlying scaling relations in the dark matter properties of the cluster. Following this line of reasoning, we now express the evolution of the ST relation in terms of the redshift evolution of these same dark matter properties.

The evolution of the dark matter scaling relations is apparent in Eqn 5. The normalization of these scaling relations changes with redshift according to the change in

ρ_{crit} and the change in the characteristic overdensity Δ of collapsed haloes. Within Einstein-de Sitter models Δ does not evolve, whereas evolution is expected in low Ω_M models. For simplicity of presentation, in the following analysis we explicitly follow only changes in ρ_{crit}, but accounting for changes in Δ would not affect our conclusions. Using $H(z) = H_0 E(z)$, we express the evolution of the mass and size scaling relations as

$$M_\Delta(T,z) = \frac{M_\Delta(T,0)}{E(z)} \text{ and } R_\Delta(T,z) = \frac{R_\Delta(T,0)}{E(z)} \quad (12)$$

where $E^2(z) = \Omega_M(1+z)^3 + (1-\Omega_M-\Omega_\Lambda)(1+z)^2 + \Omega_\Lambda$, and Ω_M and Ω_Λ are the present epoch contributions to the density parameter from matter and "dark energy", respectively. These simple evolution models are valid only for self similar evolution– i.e. in the case that distant cluster dark matter profiles are structurally similar to those of nearby clusters.

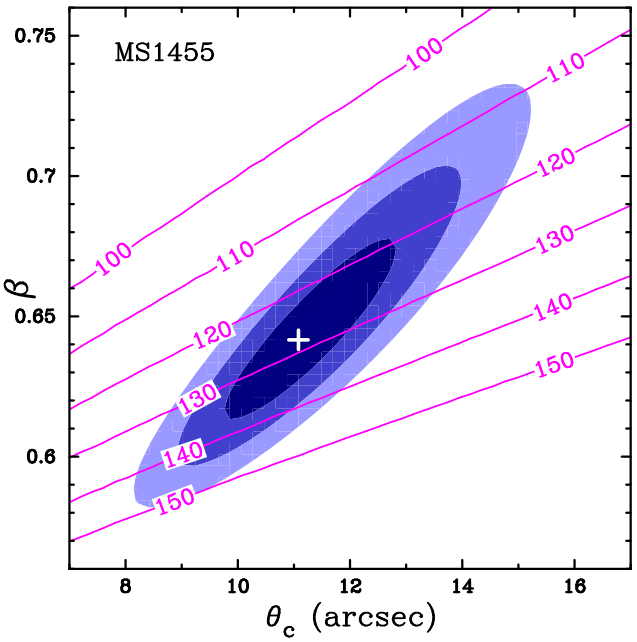

FIG. 2.— The 1, 2 and 3 σ joint confidence regions for the β model fit to MS-1455 ($\Delta\chi^2 = 2.3, 6.2, 11.8$). Overplotted are lines of constant isophotal size θ_I in arcseconds. Note that these lines run at shallow angles with respect to the β-θ_c correlation, reducing the correlation's effect on our θ_I uncertainties.

From Eqn 8 it follows that the X-ray surface brightness at R_δ evolves as $I(R_\delta) \propto E^3(z)$ and that the normalization of the ST relation evolves as

$$R_I(T,z) = R_I(T,0)\, E^\eta(z) \text{ where } \eta = \frac{4-6\beta}{6\beta-1} \quad (13)$$

Interestingly, for the most common cluster profile $\beta = 2/3$ (local: Jones & Forman 1984, Mohr, Mathiesen & Evrard 1999; this intermediate redshift sample: $\langle\beta\rangle = 0.63\pm0.04$), so $\eta = 0$, corresponding to no evolution in the ST relation. In essence, a cluster of a given T_X is denser in the past, boosting its X-ray surface brightness and tending to increase the isophotal radius R_I, but this cluster is also smaller in the past, tending to decrease the isophotal radius R_I. If the ICM density profile behaves as $\rho_g \propto r^{-2}$, these two effects cancel. Thus, a population of clusters with measured $\beta \sim 2/3$ will exhibit an ST relation which is relatively insensitive to cosmological evolution. In principle, this behavior makes the ST relation ideal for measuring angular diameter distances to high redshift clusters.

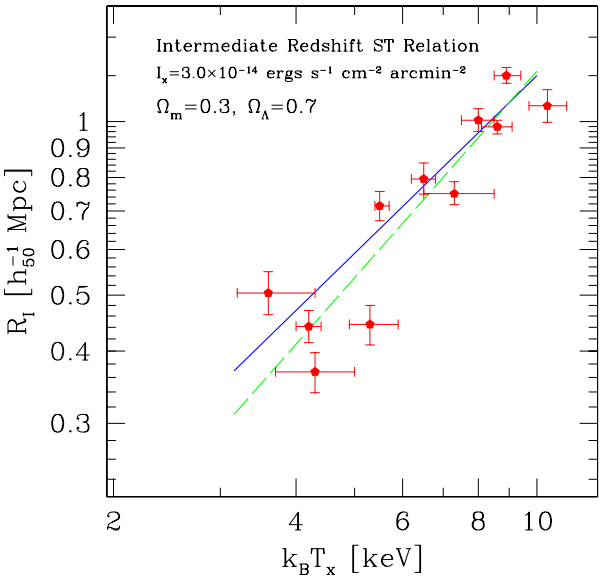

FIG. 3.— The X-ray ST relation for 11 members of the CNOC cluster sample with measured T_X. For this figure the conversion from measured $\theta_I \rightarrow R_I$ is done assuming $\Omega_M = 0.3$ and $\Omega_\Lambda = 0.7$. Error bars denote 1 σ uncertainties in emission weighted mean temperature T_X and in isophotal size R_I. The solid line is the best fit ST relation determined from the nearby cluster sample (Fig 1), and the dashed line is the best fit ST relation for the intermediate redshift sample.

3.2. *Observations*

We use archival ROSAT HRI observations of 11 of the 14 CNOC clusters discussed in Lewis et al. (1999); these 11 clusters are those with published T_X measurements. A detailed description of the reduction to 0.5″ pixel images is given in Lewis et al. (1999). The HRI angular resolution is $\sim$ 5″ FWHM; we further bin these images to a final pixel size of 2″ without significant loss of angular resolution. Despite the far higher median exposure time (33 ks compared to 8 ks), the image quality of these intermediate redshift clusters is far lower than for our nearby sample (due to combination of lower observer frame surface brightness and higher instrument background). The image quality is too poor to allow isophotal sizes measurements directly from the images using the approach described in §2; therefore, we fit circular β models (same form as Eqn 9 with θ substituted for R) to these images using the software developed for measuring SZE+X-ray distances (Reese et al. 2000). Essentially, we find the set of parameters I_0, θ_c, β, cluster centroid (α, δ) and local background I_{bkg} which maximizes the likelihood of consistency between model and data. In all these fits we fix the background to the value measured in an annulus extending from 4.5′ to 5′, a background dominated region with an essentially negligible contribution from the cluster. Fits are performed to the central portion ($\theta \leq 4.2'$) of the image which includes the cluster and a local background region. In Table 1 we list the best fit parameters with estimates of the statistical uncertainties. The central surface brightness and measured background are both given in detector

units of cts $s^{-1}arcmin^{-2}$.

These cluster parameters are in reasonably good agreement with those presented in Lewis et al. (1999), with the exception of two clusters A2390 and MS1358. The different best fit parameters in these two clusters stem from the treatment of emission excesses; we fit the surface brightness model to the entire dataset, whereas Lewis et al. (1999) exclude the central region in both these clusters. This exclusion approach typically leads to larger core radii and correspondingly higher β's than would fitting to the entire cluster as in our method.

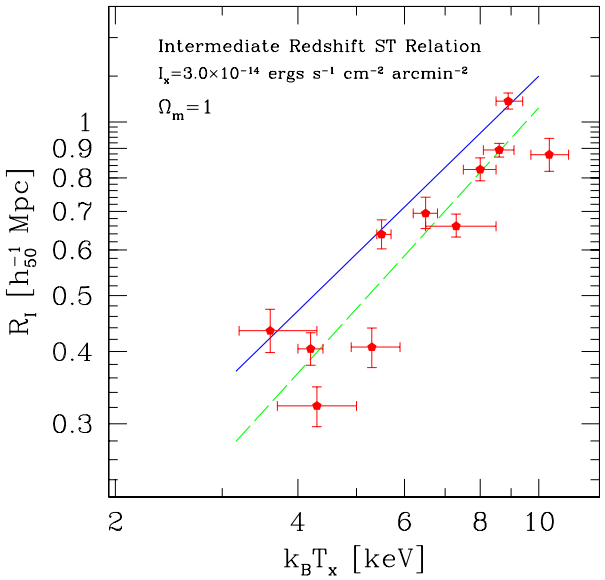

FIG. 4.— The X-ray ST relation for 11 members of the CNOC cluster sample. For this figure the conversion from measured $\theta_I \rightarrow R_I$ is done assuming $\Omega_M = 1$. Error bars denote 1 σ uncertainties in emission weighted mean temperature T_X and in isophotal size R_I. The solid line is the best fit ST relation determined from the nearby cluster sample (Fig 1), and the dashed line is the best fit ST relation for the 11 intermediate redshift clusters.

An examination of the fit residuals in our sample provides no clear evidence for systematic differences between the data and the models with the exception of A2390, which exhibits an asymmetry or centroid variation (e.g. Mohr, Fabricant & Geller 1993). Allowing for an ellipticity introduces two additional free parameters, and the information content of some of the images simply is not sufficient to provide meaningful constraints. Our goal here is to determine whether there is any evidence of regularity in intermediate redshift clusters; any mismatch between the data and the model (like that in A2390) will serve simply as an additional source of scatter in the final relation. Therefore, we conservatively present a uniform and objective analysis which is appropriate for the majority of our sample, rather than varying our analysis from cluster to cluster. (An elliptical β model fit to A2390 yields an isophotal size which is 8% smaller than that listed in Table 1. This correction makes A2390 more consistent with the best fit ST relation, but the correction is unimportant compared to the 17% RMS scatter of the sample about that best fit relation.) Of course the best approach is a non-parametric analysis of the surface brightness maps such as that applied to the local sample, but this is not possible with the current data.

We use PROS to convert the detector count rate into galactic absorption corrected flux units of ergs $s^{-1}cm^{-2}$ within the cluster rest frame 0.5:2.0 keV band. As for the low redshift clusters, we assume a Raymond-Smith emission spectrum with the measured mean temperature T_X and $\frac{1}{3}$ cosmic abundances (Mushotzky & Loewenstein 1997) at the appropriate redshift, and then we correct for the $(1+z)^4$ cosmological dimming. The rest frame 0.5:2.0 keV central surface brightnesses in units of ergs $s^{-1}cm^{-2}arcmin^{-1}$ are also listed for each cluster.

Angular isophotal sizes θ_I are then estimated using a fiducial surface brightness of 3.0×10^{-14} ergs $s^{-1}cm^{-2}arcmin^{-2}$. We determine statistical uncertainties in the fit parameters by exploring the likelihood within a grid in the parameters I_0, θ_c and β; we then use that range to estimate uncertainties in the derived isophotal size θ_I. Figure 2 contains a plot of the 1, 2 and 3σ confidence regions in β and θ_c for MS1455; lines of constant isophotal size θ_I are overlaid. Note that lines of constant θ_I are approximately parallel to the well known $\beta - \theta_c$ correlation (e.g. Mohr, Mathiesen & Evrard 1999), minimizing the detrimental effects this correlation has on our size measurement uncertainties.

Measured θ_I are then converted into physical isophotal sizes R_I using the angular diameter distance d_A: $R_I = \theta_I d_A$. We use the general form

$$d_A = \frac{c}{H_0(1+z)} \frac{F\left(\kappa \int_0^z \frac{dz'}{E(z')}\right)}{\kappa}$$
$$\kappa = \sqrt{|1 - \Omega_M - \Omega_\Lambda|} \qquad (14)$$

where $F(x) = sinh(x)$, x, and $sin(x)$ in an open, flat and closed cosmology. Table 1 contains a list of θ_I for $I_x = 3.0 \times 10^{-14}$ ergs/s/cm^2/arcmin^2 with statistical uncertainty estimates and the corresponding R_I for the case where $\Omega_M = 0.3$ & $\Omega_\Lambda = 0.7$.

Figure 3 contains the intermediate redshift ST relation with 1σ error bars in both T_X and R_I. The conversion from θ_I to R_I assumes $\Omega_M = 0.3$ and $\Omega_\Lambda = 0.7$ in this figure. The best fit relation in this case is

$$R_I = (0.67 \pm 0.04) \left(\frac{T_X}{6\,\mathrm{keV}}\right)^{1.19 \pm 0.21} h_{50}^{-1}\ \mathrm{Mpc}, \qquad (15)$$

and the RMS scatter in size about this relation is 17%. Also plotted is the local ST relation for this same isophote (solid line). The uncertainties are derived by bootstrap resampling the list of 11 sizes (allowing duplication) and refitting the relation.

There is a suggestion that the intermediate redshift ST relation is steeper than the local relation, but the difference in slopes is less than 1σ significant. In fact, both the zeropoints and slopes of the local and intermediate ST relations are statistically consistent when we use this particular set of cosmological parameters. With a larger sample it will be possible to measure the intermediate redshift ST relation slope more accurately; a comparison of the two slopes would be an important diagnostic of unusual structural evolution in clusters.

Figure 4 contains a plot of the intermediate redshift ST relation assuming $\Omega_M = 1$. The best fit slope in this case is 1.16 ± 0.20, and the zeropoint is 0.59 ± 0.034. This zeropoint differs from that of the local ST relation (also calculated with $\Omega_M = 1$) at 2.5σ.

TABLE 1
CLUSTER FIT PARAMETERS AND ISOPHOTAL SIZE

Cluster	z	k_BT_X keV	I_o[a]	I_o[b]	θ_c $''$	β	I_{bkgd}[a]	θ_I $''$	R_I[c]
A2390	0.2279	$8.9^{+0.5}_{-0.4}$	$0.159^{+0.011}_{-0.008}$	9.33	$17.2^{+1.1}_{-1.2}$	$0.532^{+0.008}_{-0.008}$	0.0022	$235.1^{+6.1}_{-5.7}$	1.202
MS0015.9+1609	0.5466	$8.0^{+0.5}_{-0.5}$	$0.018^{+0.001}_{-0.001}$	1.63	$49.4^{+5.9}_{-5.2}$	$0.898^{+0.095}_{-0.073}$	0.0020	$112.3^{+3.9}_{-3.6}$	1.005
MS0440.5+0204	0.1965	$5.3^{+0.6}_{-0.4}$	$0.079^{+0.020}_{-0.014}$	4.71	$9.1^{+2.0}_{-1.7}$	$0.521^{+0.029}_{-0.023}$	0.0023	$97.7^{+5.8}_{-5.9}$	0.445
MS0451.5+0250	0.2010	$8.6^{+0.5}_{-0.5}$	$0.012^{+0.001}_{-0.001}$	0.69	$94.6^{+4.2}_{-4.2}$	0.750	0.0024	$211.0^{+5.5}_{-5.8}$	0.979
MS0451.6-0305	0.5392	$10.4^{+0.8}_{-0.7}$	$0.025^{+0.002}_{-0.002}$	2.30	$36.4^{+5.2}_{-4.1}$	$0.752^{+0.070}_{-0.056}$	0.0023	$119.7^{+5.7}_{-5.7}$	1.064
MS0839.8+2938	0.1928	$4.2^{+0.2}_{-0.2}$	$0.129^{+0.018}_{-0.015}$	6.33	$11.9^{+1.7}_{-1.4}$	$0.588^{+0.028}_{-0.022}$	0.0023	$98.4^{+5.1}_{-4.9}$	0.442
MS1008.1-1224	0.3062	$7.3^{+1.2}_{-0.8}$	$0.018^{+0.001}_{-0.001}$	1.24	$35.8^{+4.1}_{-3.5}$	$0.667^{+0.042}_{-0.036}$	0.0023	$118.5^{+4.1}_{-3.7}$	0.745
MS1224.7+2007	0.3255	$4.3^{+0.7}_{-0.6}$	$0.054^{+0.013}_{-0.010}$	3.19	$7.5^{+1.7}_{-1.3}$	$0.552^{+0.034}_{-0.028}$	0.0025	$55.9^{+3.4}_{-3.6}$	0.368
MS1358.4+6245	0.3290	$6.5^{+0.3}_{-0.3}$	$0.111^{+0.022}_{-0.016}$	6.14	$8.4^{+1.4}_{-1.4}$	$0.501^{+0.016}_{-0.016}$	0.0023	$119.7^{+6.0}_{-5.4}$	0.795
MS1455.0+2232	0.2570	$5.5^{+0.1}_{-0.2}$	$0.460^{+0.042}_{-0.037}$	31.86	$11.2^{+1.0}_{-0.9}$	$0.643^{+0.022}_{-0.019}$	0.0028	$127.7^{+6.3}_{-6.1}$	0.713
MS1512.4+3647	0.3726	$3.6^{+0.7}_{-0.4}$	$0.107^{+0.022}_{-0.017}$	6.20	$7.4^{+1.4}_{-1.2}$	$0.560^{+0.032}_{-0.025}$	0.0022	$70.1^{+4.7}_{-4.6}$	0.505

[a] cts s^{-1}arcmin^{-2}

[b] 10^{-12} ergs s^{-1} cm^{-2} arcmin^{-2} in rest frame 0.5:2 keV band

[c] h_{50}^{-1} Mpc for $\Omega_M = 0.3$ and $\Omega_\Lambda = 0.7$

We have examined the local and intermediate redshift ST relations at four other isophotes: 1.5×10^{-14} cgs, 2.0×10^{-14} cgs, 4.0×10^{-14} cgs, and 5.0×10^{-14} cgs. The general conclusions reached above using the isophote 3.0×10^{-14} cgs apply equally as well at these other isophotes: there is a suggestion that the ST relation at intermediate redshift is steeper (at less than 1 σ significance) than the local relation, and the zeropoints are in good agreement when using the cosmological parameters $\Omega_M = 0.3$ and $\Omega_\Lambda = 0.7$. The fainter the isophote the larger the enclosed region. Pushing to fainter isophotes is dangerous given the quality of the intermediate redshift data, and pushing to brighter isophotes leads to complications from central emission excesses and the effects of the PSF. Thus, we choose the isophote 3.0×10^{-14} cgs as a compromise between these two competing effects.

3.3. *Cosmological Constraints*

Although the X-ray images of these 11 clusters are poor, it is nevertheless interesting to use the local ST relation and our evolution model to predict distances to the intermediate redshift sample, thereby constraining cosmological parameters. Because the clusters are at a range of redshifts, both the scatter of the data about the local ST relation and any systematic offsets from the local relation contain cosmological information. Operationally, for each set of cosmological parameters Ω_M and Ω_Λ we convert the measured $\theta_I \rightarrow R_I$ and calculate the χ^2 of the sample about the best fit local ST relation, where the best fit local relation is calculated using this same set of cosmological parameters. Fig 5 contains contours of $\Delta\chi^2$ corresponding to 1, 2 and 3 σ confidence regions (equivalent to $\Delta\chi^2 = 2.3$, 6.2 and 11.8) in the Ω_M–Ω_Λ space.

The current sample, because of observational uncertainties, does not provide a strong cosmological constraint. The 1σ confidence region is a wide trough similar in character to those derived from luminosity distances to SNe Ia (Schmidt et al. 1998, Perlmutter et al. 1999), with the important difference that our sample of 11 intermediate redshift distances is not as constraining as the larger samples of SNe Ia distances. Notably, there is enough power in the current dataset to exclude the $\Omega_M = 1$ & $\Omega_\Lambda = 0$ model (one of three models marked with stars) at >95% confidence. If one considers only models where $\Omega_M + \Omega_\Lambda = 1$, then the preferred model has $\Omega_M = 0.09$. Furthermore, $\Omega_M < 0.32$ with 1σ confidence and $\Omega_M < 1$ with 3σ confidence.

One can also use these data to constrain the deceleration parameter $q_0 \equiv \Omega_M - \Omega_\Lambda/2$. The preferred value is $q_0 = 0.11^{+0.41}_{-0.65}$ (68% confidence).

Clearly, larger samples of archival data and the impending stream of high quality X-ray images from Chandra and XMM will provide tighter constraints. One particular concern in this study is that the local and intermediate redshift samples were observed with two different instruments: the ROSAT PSPC and the ROSAT HRI. Any relative calibration errors would then serve to bias the preferred cosmological parameters. However, the steepness of cluster X-ray surface brightness profiles mitigates this potential problem; typically, the surface brightness falls off as $I \propto \theta^{-3}$, so even a 10% relative error in the calibration of the PSPC and HRI would introduce only a 3% error in the angular size of the cluster.

Although there has been no previous use of cluster scaling relations to constrain cosmological parameters, there have been three attempts to use the ICM mass fraction f_{ICM} (Pen 1997, Cooray 1998, Rines et al 1999); if one assumes f_{ICM} is constant with redshift, then one can use its distance dependence to constrain the distance–redshift relation. The Pen constraint $q_0 = 0.89 \pm 0.29$ is marginally

inconsistent with our measurement, but the Pen analysis is only appropriate in the case that the ICM traces the dark matter, a case that is inconsistent with both theoretical and observational studies (David, Jones & Forman 1995, Evrard 1997).

In the Rines et al. analysis, care is taken to (1) match the luminosity ranges of the local and intermediate redshift samples, (2) address the expected radial variation of f_{ICM}, and (3) test the consistency of the published effective areas of the two satellites involved (Einstein and ASCA). Because f_{ICM} increases slowly with radius, it is important that it be measured within the same portion of the virial region in the local and intermediate redshift samples; this complicates the use of f_{ICM} measurements as cosmological constraints. If one analyzes local and intermediate redshift clusters at a fixed metric aperture, the region studied will correspond to a larger fraction of the virial region as the redshift increases (see Eqn. 12). Similarly, when measuring f_{ICM} within a fixed portion of the virial region r_{500}, it is important that the redshift evolution of the $r_{500} - T_x$ be included; it appears that in both the Rines et al. and Cooray analyses, no evolution was included, so the portion of the virial region used in determining f_{ICM} increases with redshift. In both cases, these biases cause the inferred angular diameter distances to be underestimated.

The size of the bias depends on the cosmological model being evaluated (Eqn. 12); using the relation $f_{ICM} \propto d_A^{3/2}(r/r_{500})^{0.15}$ (Evrard 1997, Pen 1997), we estimate the bias on d_A at $z = 0.35$ to be -2% for $\Omega_M = 0.3$ & $\Omega_\Lambda = 0.7$, and -10% for $\Omega_M = 1$ and $\Omega_\Lambda = 0$; these biases are important relative to the $\sim$8% difference in $d_A(z = 0.35)$ between an $\Omega_M = 0.3$ and an $\Omega_M = 0.3$ & $\Omega_\Lambda = 0.7$ cosmology. Correcting for this bias will improve the consistency between our cosmological constraints and those of Rines et al. and Cooray.

4. CONCLUSIONS

We present the local X-ray Size–Temperature (ST) relation for an X-ray flux limited sample of 45 clusters observed with the ROSAT PSPC (Mohr & Evrard 1997). We provide an explanation of this scaling relation in terms of underlying scaling relations in the cluster dark matter properties. The observed ST relation is slightly steeper than the self–similar expectation presented in §2.3, but is consistent when the modest variation of the ICM mass fraction f_g with T_x is taken into account (Mohr, Mathiesen & Evrard 1999).

We use our theoretical model for the ST relation to explore its evolution with redshift. Interestingly, for the typical ICM radial distribution observed in nearby and distant clusters, the normalization of the ST relation is not expected to evolve. The lack of evolution makes the ST relation a plausible source of intermediate redshift angular diameter distances. Of course, if cluster structure evolution is very different from the current theoretical expectation, our model (§3.1) will underestimate ST relation evolution. For example, a shift in the mean ICM mass fraction with redshift would bias ST relation distances; to date there is no compelling evidence that distant clusters have different ICM mass fractions in the mean than nearby clusters (e.g. Lewis et al. 1999, Grego et al. 2000).

We use ROSAT HRI observations of 11 CNOC clusters with measured emission weighted mean ICM temperatures T_X to make the first measurements of the intermediate redshift ST relation. Because of the poor image quality, we measure the angular isophotal size θ_I using the best fit circular β model, rather than measuring it nonparametrically as for the nearby clusters (see Eqn 1). By assuming the cosmological parameters $\Omega_M = 0.3$ & $\Omega_\Lambda = 0.7$, we show that the slope and zeropoint of this intermediate redshift ST relation is statistically consistent with that of the local ST relation (see Fig 3). In addition, we examine the relation for $\Omega_M = 1$ & $\Omega_\Lambda = 0$ (see Fig 4), showing that although the slope is consistent, the zeropoint is different at greater than 3σ significance.

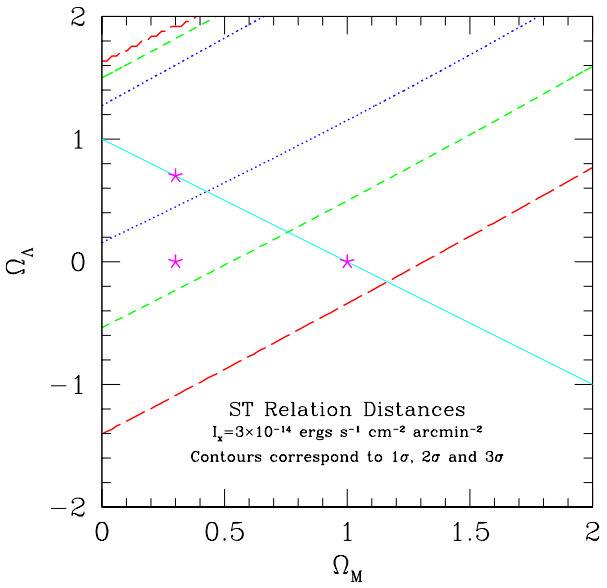

FIG. 5.— Cosmological constraints from X-ray ST relation distance measurements to 11 intermediate redshift clusters. Contours correspond to 1, 2 and 3 σ confidence regions ($\Delta\chi^2 = 2.3$, 6.2 and 11.8). The solid line marks spatially flat models, and the stars mark models $\Omega_M = 0.3$ & $\Omega_\Lambda = 0.7$, $\Omega_M = 0.3$ and $\Omega_M = 1$.

Finally, we use this cluster sample and our ST relation evolution model to place cosmological constraints. Given the quality of the cluster images and temperature measurements, it is not surprising that a wide range of cosmological models is consistent with the data. Nevertheless, this sample of 11 intermediate redshift distances is sufficient to rule out $\Omega_M = 1$ with between 2σ and 3σ confidence. Taken together with ICM mass fraction constraints on the cosmological matter density parameter $\Omega_M < 0.44$ at 95% confidence (Mohr, Mathiesen & Evrard 1999), the cluster ST relation exhibits a slight preference for universes with $\Omega_\Lambda > 0$; models with $\Omega_\Lambda = 0$ are inconsistent with the ST relation at between 1 and 2σ. When considering only models where $\Omega_M + \Omega_\Lambda = 1$, we can rule out $\Omega_M = 1$ with 3σ confidence.

With the higher quality X-ray images and ICM temperature measurements available from Chandra and XMM, a significant tightening of these constraints and further tests of the underlying evolution model will be possible. Comparison of local and distant $M_{ICM} - T_X$ relations, which are more sensitive to cluster evolution, would provide important constraints on these models. In addition, observations with a new generation of Sunyaev-Zel'dovich effect instruments (Carlstrom et al. 1999, Mohr et al.

1999, Holder et al. 2000) will allow us to more accurately constrain the evolution of cluster structure. With these future observations of intermediate and high redshift clusters, we plan to continue using the ST relation as a tool to provide cosmological constraints independent of those derived from recent high redshift SNe Ia observations (Schmidt et al. 1998, Perlmutter et al. 1999).

JJM is supported by Chandra Fellowship grant PF8-1003, awarded through the Chandra Science Center. The Chandra Science Center is operated by the Smithsonian Astrophysical Observatory for NASA under contract NAS8-39073. EDR is supported by NASA GSRP Fellowship NGT5-50173. EE acknowledges support provided by the National Science Foundation grant AST 9617145. AEE acknowledges support from NSF AST-9803199 and NASA NAG5-8458. This research has made use of data obtained through the High Energy Astrophysics Science Archive Research Center Online Service, provided by the NASA/Goddard Space Flight Center.

REFERENCES

Arnaud, M. & Evrard, A.E. 1999, MNRAS, 305, 631
Bryan, G.L. & Norman, M.L. 1998, ApJ, 496, 80
Buote, D.A. & Tsai, J.C., 1996, ApJ, 458, 27
Carlstrom, J.E., Joy, M.K., Grego, L., Holder, G.P., Holzapfel, W.L., Mohr, J.J., Patel, S. & Reese, E.D. 1999, contribution to Nobel Symposium on Particle Physics and the Universe, astro-ph/9905255
Cavaliere, A. & Fusco-Femiano, R. 1978, A&A, 70, 677
Cavaliere, A., Menci, N. & Tozzi, P. 1998, ApJ, 501, 493
Cooray, A.R. 1998, A&A, 333, L71
David, L.P., Slyz, S.C., Forman, W., Vrtilek, S.D. & Arnaud, K.A. 1993, ApJ, 412, 479
David, L.P., Jones, C. & Forman, W. 1995, ApJ, 445, 578
Edge, A.C., Stewart, G.C., Fabian, A.C. & Arnaud, K.A. 1990, MNRAS, 245, 559
Evrard, A.E., Metzler, C.A. & Navarro, J.F. 1996, ApJ, 469, 494
Evrard, A.E. 1997, MNRAS, 292, 289
Fabian, A.C., Crawford, C.S., Edge, A.C. & Mushotzky, R.F. 1994, MNRAS, 267, 779
Fabricant, D., Lecar, M. & Gorenstein, P. 1980, ApJ, 241, 552
Grego, L., Carlstrom, J.E., Reese, E.D., Holder, G.P., Holzapfel, W.L., Joy, M.K., Mohr, J.J., & Patel, S. 2000, ApJ, submitted
Holder, G.P., Mohr, J.J., Carlstrom, J.E., Leitch, E.M. & Evrard, A.E. 2000, ApJ, in press (astro-ph/9912364)
Horner, D.J., Mushotzky, R.F. & Scharf, C.A. 1999, ApJ, 520, 78
Jones, C. & Forman, W.F. 1984, ApJ, 276, 38
Jing, Y.P. & Suto, Y. 1999, (astro-ph/9909478)
Jørgensen, I., Franx, M. & Kjærgaard, P. 1996, MNRAS, 280, 167
Lewis, A.D., Ellingson, E., Morris, S.L. & Carlberg, R.G. 1999, ApJ, 517, 587
Markevitch, M. 1998, ApJ, 504, 27
Metzler, C.A. & Evrard, A.E. 1994, ApJ, 437, 564
Mohr, J.J., Fabricant, D.G. & Geller, M.J. 1993, ApJ, 413, 492
Mohr, J.J., Evrard, A.E., Fabricant, D.G & Geller, M.J. 1995, ApJ, 447, 8
Mohr, J.J. & Evrard, A.E. 1997, ApJ, 491, 13
Mohr, J.J., Mathiesen, B. & Evrard, A.E. 1999, ApJ, 517, 627
Mohr, J.J., Carlstrom, J.E., Holder, G.P., Holzapfel, W.L., Joy, E.M. & Reese, E.D. 1999, "VLT Opening Symposium", (astro-ph/9905256)
Moore, B., Quinn, T., Governato, F., Stadel, J. & Lake, G. 1999, MNRAS, 310, 1147 (astro-ph/9903164)
Mushotzky, R.F. & Loewenstein, M. 1997, ApJ, 481, L63
Navarro, J.F., Frenk, C.S. & White, S.D.M. 1997, ApJ, 490, 493
Pen, U. 1997, New Astronomy, 2, 309
Perlmutter, S. et al. 1999, ApJ, 517, 565
Ponman, T.J., Cannon, D.B. & Navarro, J.F. 1999, Nature, 397, 135
Raymond, J.C. & Smith, B.W. 1977, ApJS, 35, 419
Reese, E.D., Mohr, J.J., Carlstrom, J.E., Joy, M., Grego, L., Holder, G.P., Holzapfel, W.L., Hughes, J.P., Patel, S. & Donahue, M. 2000, ApJ, 533, 38 (astro-ph/9912071)
Rines, K., Forman, W., Pen, U., Jones, C., Burg, R. 1999, ApJ, 517, 70
Schmidt, B.P. et al. 1998, ApJ, 507, 46
Yee, H.K.C., Ellingson, E., & Carlberg, R.G. 1996, ApJS, 102, 269